Variances of momentum and heat fluxes over turbulence generated by cube array in convective boundary layer

Number: 3A.7

Yuya Baba*, Keiko Takahashi
*Earth Simulator Center (ESC),
Japan Agency for Marine-Earth Science and Technology (JAMSTEC)
3173-25 Showa-machi, Kanazawa-ku, Yokohama, 236-0001 Japan

1. INTRODUCTION

Convective boundary layer (CBL) is one of the states of planetary boundary layer (PBL), and the PBL in this state takes an important role for generating momentum and heat fluxes from the ground or sea surfaces. CBL over complex geometry is known to have variety of turbulence structures, and the variations of both momentum and heat fluxes depend on the ground surface geometry.

In some previous studies, turbulence structure over regular cube array has been studied assuming neutrally stratified atmospheric condition, and those studies revealed that some important features of turbulence, for instance, the turbulent flow has organized large-scale structures (e.g., Kanda et al. 2004). However, the previous studies didn't discuss the interaction mechanism between the turbulence structure and heat transfer. This issue has been investigated by experimental approaches, but flow structure is analyzed by only statistics (e.g., Uehara et al. 2000). This interaction mechanism might become important for capturing the CBL's features over complex geometry and those roles in the atmosphere, since the heat transfer causes vertical thermal convection, which also causes small- and large-scale interaction between outer and inner layers of boundary layer.

We will focus on the interaction mechanism between turbulence structure and heat transfer by investigating variances of momentum and heat fluxes (heat flux is regarded as buoyancy flux in this study). In order to investigate and discuss this issue, we chose idealized setting similar to the previous studies which analyzed canopy turbulence, but we impose surface heat flux at the bottom wall.

2. MODEL DESCRIPTIONS

The governing equations of our model consist of mass, momentum and energy conservation equations given as (see more detail in Moureau et al. (2007))

$$\frac{\partial \rho}{\partial t}+\frac{\partial \rho u_j}{\partial x_j}=0\,, \tag{1}$$

$$\frac{\partial \rho u}{\partial t}+\frac{\partial \rho u_i u_j}{\partial x_j}+\rho g\delta_{i3}=-\frac{\partial P}{\partial x_i}-\frac{\partial \tau_{ij}}{\partial x_j}-\rho\varepsilon_{ij3}\left(u_j-U_j^g\right), \tag{2}$$

$$\frac{\partial \rho h}{\partial t}+\frac{\partial \rho u_j h}{\partial x_j}=\frac{\partial P}{\partial t}+u_j\frac{\partial P}{\partial x_j}-\tau_{ij}\frac{\partial u_i}{\partial x_j}-\frac{\partial \tau_{hj}}{\partial x_j}\,. \tag{3}$$

This compressible formulation is useful for simulating upper stable atmospheric boundary layer, mixing layer and unstable surface layers simultaneously, and considering density stratification which has great influence on vertical evolution of the CBLs (Baba & Takahashi (2010)).

Discretization for the governing equations is done with 2nd-order finite difference method on the staggered grid. Nonlinear terms of the compressible Navier-Stokes equations are computed from fully conservative skew-symmetric scheme of Morinishi (2009), whereas 3rd-order upwind scheme, QUICK is used for scalar advection terms (as for the use of QUICK, see Baba & Kurose 2008). Time integration is performed by 2nd-order Adams-Bashforth method. A subgrid scale model of Deardorff (1980) is used to model the turbulence. To solve the set of governing equations, compressible solver proposed by Moureau et al. (2007) is applied. The model validity has been preliminarily confirmed by comparing our results with those of Uehara et al. (2000).

3. EXPERIMENTAL SETUP

Our experimental setup follows to the idealized setting similar to those used in Kanda et al. (2004) and Kanda (2006). The computational domain of this study is illustrated in Fig.1. Cube array, which have $\mathrm{H}=50$ m height and $\mathrm{H}\times\mathrm{H}$ square, are arranged with equal spacing at the bottom of the computational domain. The number of cube arrays is changeable and varies with the domain size defined by $\mathrm{L_X}\times\mathrm{L_Y}$. To explicitly resolve the cube array, 5 m horizontal resolution is used. In the vertical direction, nonuniform grid spacing is used, where the highest resolution is 5m near the wall, and grid spacing is set to become larger toward top of the domain.

Table 1 summarizes all simulation cases. Large organized motion is known to appear over the cube array as shown in Kanda et al. (2004). In addition, much more

larger organized structure is expected to appear in the CBL, which will be induced by thermal convection. Therefore sensitivity of the result to the computational domain size will be important to capture all dominant scales of the CBL, and different domain sizes are chosen to investigate this domain size effect. Horizontal domain size is changeable while fixed vertical height up to 2 km is considered in the all cases.

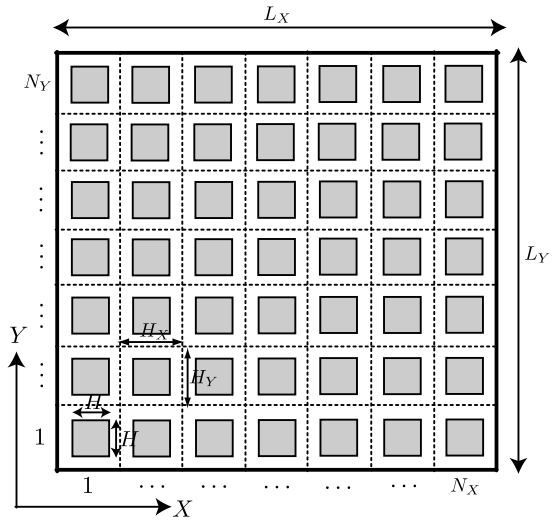

Figure 1: Geometrical arrangement of cube array.

Different stability conditions of the boundary layers are also considered aiming at investigating structure variations of turbulence. Three conditions, namely stable, neutral and convective conditions are set by imposing different bottom wall temperature (301 K, 305 K), and different geostrophic wind speed (4 m/s, 8 m/s). In the present study, domain center latitude is set to be 35^{O}N, namely mid-latitude.

Initial and background potential temperature profiles are given to take the buoyancy, gravity forces and density stratification into account. Figure 2 shows the vertical profiles for both initial and background fields. Statistically unstable condition is assumed under 100 m height which is regarded as surface layer, while neutral and stable conditions are assumed for from 100 m to 1000 m heights, and higher than 1000 m, respectively. If the potential temperature profile is determined, other fields such as density, temperature and pressure fields are automatically determined using the equation of hydrostatic relation.

Table 1: All simulation cases.

Case	Domain size	Stability
Run-LS	3km x 3km	Stable
Run-MS	2km x 2km	Stable
Run-SS	1km x 1km	Stable
Run-LN	3km x 3km	Neutral
Run-MN	2km x 2km	Neutral
Run-SN	1km x 1km	Neutral
Run-LC	3km x 3km	Convective
Run-MC	2km x 2km	Convective
Run-SC	1km x 1km	Convective

4. RESULTS AND DISCUSSION

4.1. General features

Figure 3 shows horizontal distributions of wind speed at 1.2z/H height in the all cases, where z is the height and H is height of the cube unit. It is found that flow structures become larger as the PBL's condition becomes unstable. It is also found that flow direction differs in each case. This is because flow field is dominated by Coriolis force in the stable condition which streamwise wind speed is large, while the flow field's direction in neutral and convective cases are parallel to original streamwise direction, probably due to the fact that vertical evolution in these cases weaken streamwise wind speed. This trend agrees with the fact that when the wind speed is small, Coriolis force becomes small.

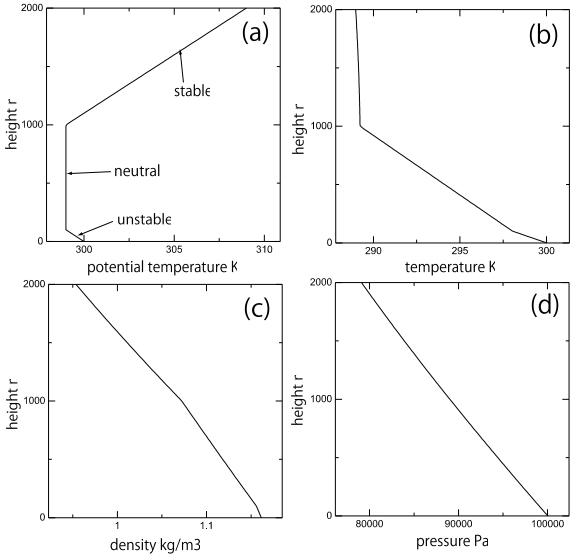

Figure 2: Vertical profiles for initial and background fields.

Comparing the results of different domain sizes, it is found that the structure of large domain size seems to consist of that of small domain size. In the stable and neutral conditions, flow features are basically similar each other, but convective cases are different. This is because flow structure of the convective case is larger than those of former two cases, due to the existence of strong vertical convection. Details of the results computed by small domain might be different from those of large domain size. This point will be discussed later.

Figure 4 shows horizontally averaged vertical distributions of r.m.s of horizontal and vertical wind speeds. The profiles of r.m.s of horizontal wind speeds (u_{rms}, v_{rms}) are similar each other, but vertical fluctuation becomes larger as the bottom wall temperature increases. In the convective case, the large fluctuation reaches nearly at the

top of the PBL. On the other hand, vertical fluctuation is seen at the upper atmosphere in the stable cases, but it is considered to be caused by stress occurring between streamwise flow and the inversion capping which is set at upper atmosphere in order to absorb gravity waves. Comparing the results of different domain size, it is also found that each case shows little differences, but difference slightly becomes large in the convective case. Therefore, the effect of domain size difference is considered to have influence in the only convective cases.

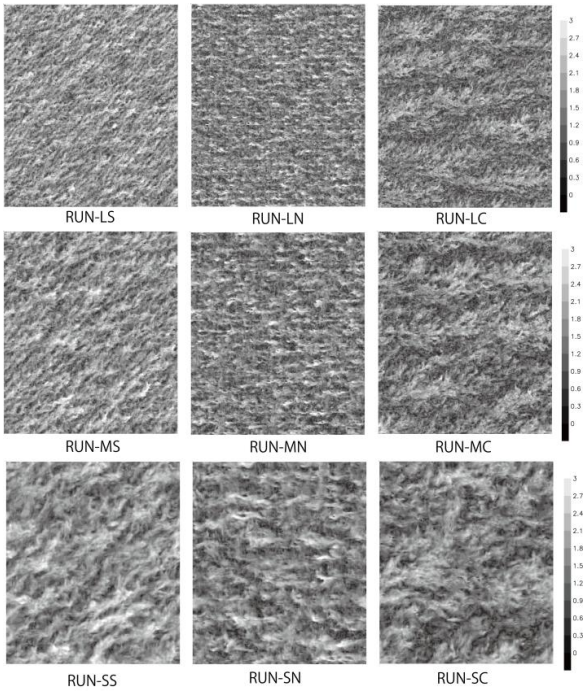

Figure 3: Horizontal wind speed ($\sqrt{u^2+v^2}$ m/s) distributions at $1.2z/H$ height.

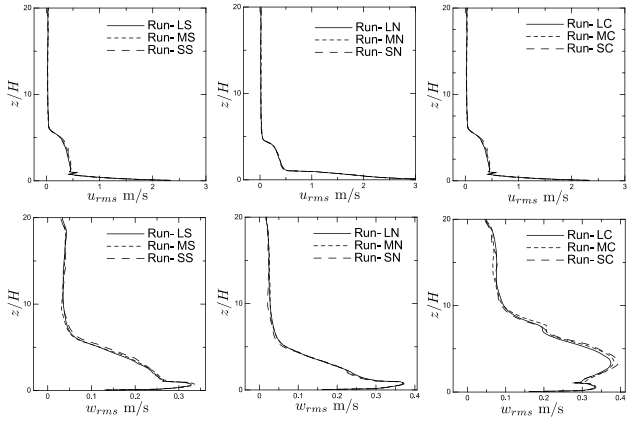

Figure 4: Vertical distributions of r.m.s of horizontal and vertical wind speeds.

Domain size effect on the turbulence structure is investigated using filtering analysis. Low-pass filter is known to be able to remove small structure of the turbulence (Tompkins & Adrian (2003); Coceal et al. (2007)), thus if the low-passed motion shows difference, it will be recognized as the effect of domain size difference. The filtered r.m.s. profiles are compared in Fig.5.

In the small domain, fluctuations are found to be overestimated at the 2.5z/H height. This is because the whole flow fields in the small domain are considered to perturb, and it is considered to be caused by ignoring the large-scale background fields. Therefore, difference of domain size has an influence on the large-scale perturbation and the effect might cause overestimation of the flow fields' fluctuation.

In addition to the domain size effect, comparing the filtered and original profiles, other features of the PBLs are found from the Fig.5. The both profiles are similar and show little difference in the u_{rms} for all heights, however, v_{rms} and w_{rms} show large differences especially from top of the cube arrays to higher than 2.5z/H. The fact indicates that small-scale structure is dominant in these regions and the dominance shits to large-scale as the height increases. In the latter discussions, results of large domain size will be basically used.

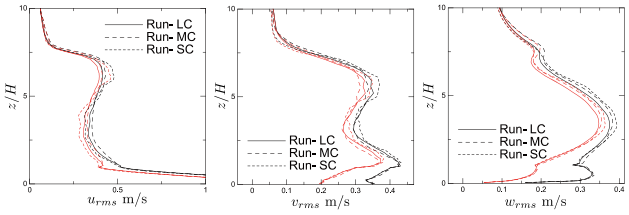

Figure 5: Vertical profiles of r.m.s. of streamwise (u_{rms}), spanwise (v_{rms}) and vertical wind speeds (w_{rms}). Black lines: original fields, red lines: low-pass filtered fields.

4.3. Turbulence structures

It is known that streak structure appears in the turbulent flow over cube array, and the structure is similar to the ordinary wall turbulence. However, the streak structure is also known to take variety of pattern depending on the surface geometry, namely the arrangement pattern of the cube array. The structure variations have been mainly studied in the past studies assuming neutral condition, but we will focus on here structure variation due to the difference of the PBL conditions with fixed cube arrangement. Variations of the streak structure in the present study are summarized in Fig.6. The structures are visualized by two low and high wind speed ranges, namely $u < 0.8u_m$ and $u > 1.2u_m$, which stand for low and high momentum regions, respectively. Here, u_m is the average horizontal wind speed.

It is found that flow field structure becomes larger as the PBL becomes unstable. Ordinary streak structure is observed in the Run-LS. In the Run-LN, wind speed difference between low and high wind speed regions becomes larger than that of Run-LS. The wind speed difference is judged from the shape boundary

among the low and high speed regions. In addition to this point, vertical structure becomes higher than that of Run-LS. The structure of Run-LC is much larger than those of former two cases. Very large turbulence structure in the horizontal distribution and vertical structure in the vertical direction are observed. The measured scale of horizontal and vertical structures is about 10H. From these visualizations, it is considered that vertical structure becomes dominant, and along with the vertical motion, horizontal structure also becomes larger in the convective case.

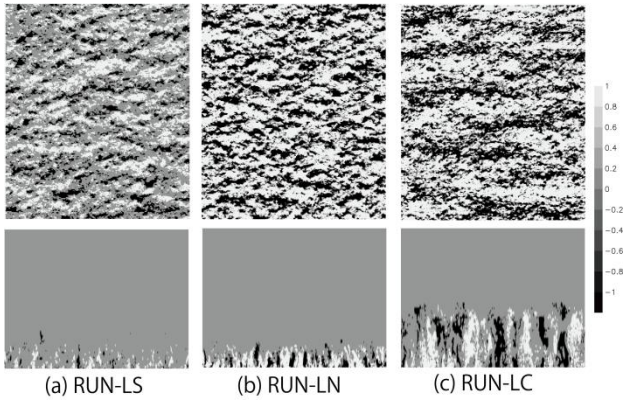

Figure 6: Low and high wind speed regions in the all large domain cases. Upper and lower figures indicate horizontal (at 1.67z/H height) and vertical structures (1.67z/H to 20z/H m height), respectively. Black region: $u < 0.8u_m$, white region: $u > 1.2u_m$.

To further investigate the turbulence structure, quadrant analysis is next performed as done in the Coceal et al. (2007). Counts of Q2 (ejection) and Q4 (sweep) events are useful for discussing interaction mechanism between lower and upper atmosphere. Q2 and Q4 events represent ejection of fluid from lower to upper levels, and sweep from upper to lower levels, respectively. Figure 7 shows the comparison of Q2 and Q4 events counts in the vertical direction. Here, event counts are normalized by the total number of grid points. Counts of Q2 and Q4 are reversed at the height of cube array's top in the Run-LC and Run-LS, but the height of Run-LN differs from those of two cases. The Run-LN and Run-LC trends mean that vertical evolution of Run-LN depends on the fluid motion, whereas that of Run-LC depends on thermal convection, which cannot be categorized into Q2 and Q4 events. On the other hand, increase of Q2 and Q4 counts in the Run-LN can be explained as vertical evolution is not suppressed compared to the Run-LS due to the neutral condition.

4.5. Flux variations

Flux variations are investigated in terms of the turbulence structure. The variation of turbulence structure is considered to depend on the variation of buoyancy flux. Figure 8 shows the horizontally averaged vertical distribution of buoyancy flux, $\overline{w'\theta'}$. The negative buoyancy flux is seen just above the top of cube array in the all cases. Increase of Q4 sweep events at z/H=1 seen in Fig.7 corresponds to this trend. As the height increases, buoyancy flux shows positive value in all cases. However, stable and neutral conditions do not show large flux, since positive buoyant forces are weakened in these two cases due to low wall bottom temperature. Thermal convection is strong in the convective case, thus the vertical profile of buoyancy flux is similar to the typical profile of the CBL. The CBL height can be defined by height where the negative buoyancy force appears, i.e. 7.4*z/H height.

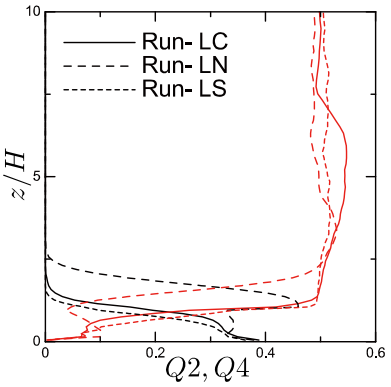

Figure 7: Vertical distribution of Q2 and Q4 events' counts. Black lines: Q2 event counts, red lines: Q4 event counts.

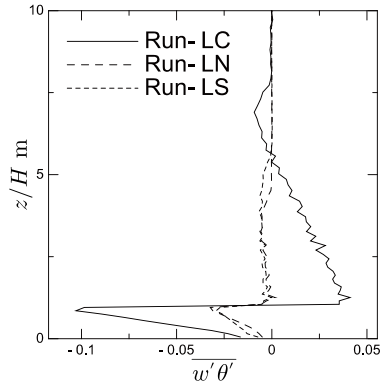

Figure 8: Horizontally averaged vertical distribution of buoyancy flux.

As already described for the Fig.6, organized large-scale structure is seen in the horizontal wind speed fields. The structure is considered to be derived from the buoyancy flux variation. To investigate relation between buoyancy flux and turbulence structure, we compared the buoyancy flux distributions for all cases (all cases are not shown). It is found that only buoyancy flux distribution of Run-LC is heterogeneous. Therefore here we describe the relation of buoyancy fluxes with other fluxes for Run-LC in detail.

Horizontal distributions of momentum fluxes, vertical wind speed and buoyancy fluxes are compared in Fig.9. In the Fig.9, all flux distributions are related each other. Momentum fluxes, vertical wind speed essentially

show positive value at the inside region of large-scale streak-like structure. However, the distribution at the edge of streaks is different for each flux. $u'w'$ flux shows slightly larger positive value, and $v'w'$ flux shows both positive and negative values simultaneously at the center of the streaks. These features of momentum fluxes mean that very large-scale streak-like structure involves vertical convection which upward motion begins from the center line of the streak-like structure.

In order to clarify the relation between fluxes, and to measure the scales of the vertical convective structures, streamwise averaged momentum and buoyancy fluxes at 1.67z/H height are computed and compared in Fig.10. Scale of buoyancy flux in the spanwise direction is about $10H$ which is about 10 times as large as the cube array length. The buoyancy flux distribution is strongly connected with large-scale structure of the flow field seen in the Fig.6. Momentum fluxes basically follows to the buoyancy flux, but $u'w'$ and $v'w'$ fluxes show different trends, when the buoyancy flux increases or decreases. Magnitude of $u'w'$ flux increases when that of buoyancy flux increases, but $v'w'$ flux sometimes does not. This fact implies that buoyancy flux acts to increase the streamwise momentum flux rather than the spanwise momentum flux. However, behavior of $v'w'$ flux partially follows to the buoyancy flux, so buoyancy might have contribution on the increase, and it agrees with the features seen in Fig.9 as the vertical convection.

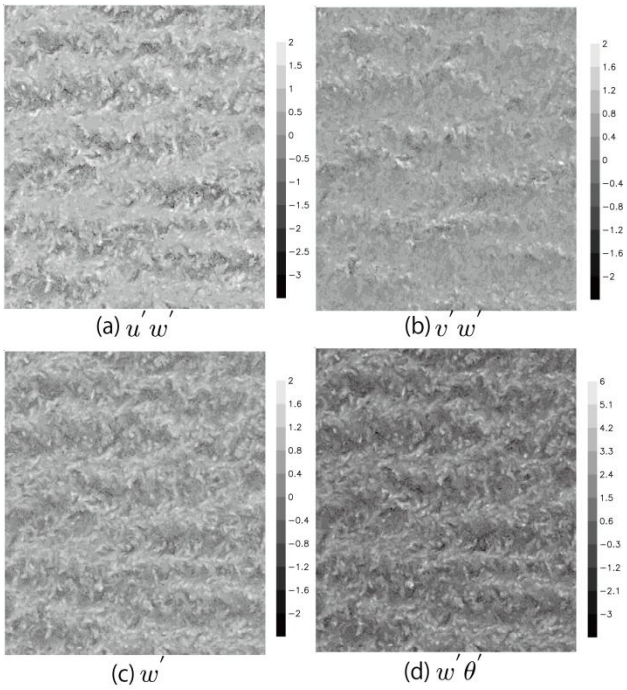

Figure 9: instantaneous horizontal distributions of momentum fluxes ($u'w', v'w'$), vertical wind speed (w') and buoyancy fluxes ($w'\theta'$) at 1.67z/H height.

5. SUMMARY AND CONCLUSION

Large-eddy simulation of convective boundary layer (CBL) involving cube array is performed, and the variances of momentum and heat fluxes are investigated in terms of turbulence structure.

General features are first shown. Coriolis force effect strongly appears in the stable condition, where geostrophic wind speed is set to be strong. As the condition becomes unstable, the Coriolis force effect disappears due to the fact that streamwise wind speed is weakened by vertical convection, and large-scale structure begins to be observed depending on the PBL's condition.

Effect of domain size difference is investigated by comparing vertical profiles of wind speed fields. Vertical distributions of wind speed fields in the all cases are not so much affected by domain size difference. Filtering analysis shows that fluctuating fields of small domain are affected by domain size difference, which background field is considered to perturb. The filtering analysis also reveals that small-scale structure is dominant up to the location higher than 2.5z/H, and large-scale becomes dominant from the location.

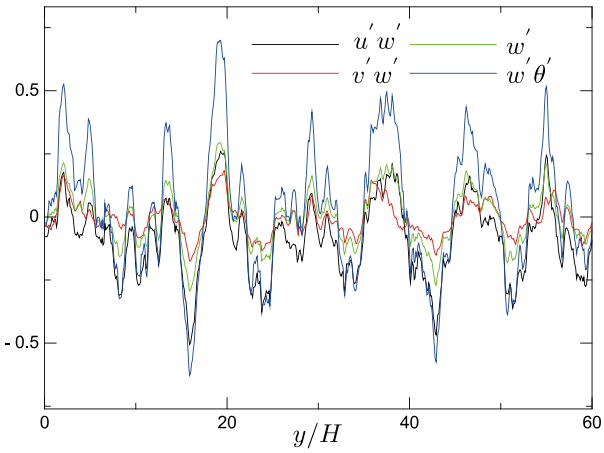

Figure 10: Spanwise distributions of streamwise averaged momentum fluxes ($u'w', v'w'$), vertical wind speed (w'), and buoyancy fluxes ($w'\theta'$) at 1.67z/H height.

Turbulence structure is investigated by analyzing streak (or streak-like) regions. Low and high momentum regions are observed, and difference between low and high wind speeds becomes larger as the PBL's condition becomes unstable. In addition to the wind speed difference, streaks also show variations. The horizontal and vertical scales of the convective condition are found to be very large and 10 times as large as the one cube unit length. Quadrant analysis is performed for the vertical direction. Counts of Q2 and Q4 events are reversed at the height of top of the cubes. Counts of each event increases as the PBL becomes unstable, but if the PBL is convective, the event counts decreases. This is because momentum exchange is conducted by thermal convection rather than fluid motion, thus when the thermal convection is dominant, quadrant analysis is not applicable.

Finally, fluxes' variations or variances along with the turbulence structure are investigated. Horizontal distributions of momentum and buoyancy fluxes are compared, and the comparison reveals that both momentum and buoyancy fluxes relate each other, and the most of the fluxes indicate positive value in the large-scale streak-like regions. However, momentum fluxes show different trends when magnitude of buoyancy flux increases. The buoyancy flux increases streamwise momentum flux, but does not always increase spanwise momentum flux. Summarizing the analysis on the flux variation, very large-scale streak-like structure is considered to involve vertical thermal convection.

When the bottom wall temperature increases more than that of the present case (5K in the present cases), the scale of turbulence structure is expected to become larger. In such situation, boundary layer should be solved so that it can capture the inner and outer layers with large-scale atmospheric motion. Coupling with atmospheric general circulation model (AGCM) or simply high resolution simulation using AGCM (involving regional model, e.g. Baba et al. 2010) will be useful for simulating such CBLs involving very large-scale atmospheric motions.

REFERENCES

Baba, Y., Takahashi, K., Sugimura, T., Goto, K., 2010: Dynamical core of an atmospheric general circulation model on a Yin-Yang grid, Mon. Wea. Rev., in press.

Baba, Y., Takahashi, K., 2010: Large-eddy simulation of convective boundary layer with density stratification, J. Meteorol. Soc. Jpn., submitted.

Baba, Y., Kurose, R., 2008: Analysis and flamelet modeling for spray combustion, J. Fluid Mech., 612, 45-79.

Coceal, O., Dobre, A., Thomas, T. G., Belcher, S. E., 2007: Structure of turbulent flow over regular arrays of cubical roughness, J. Fluid Mech., 589, 375-409.

Deardorff, J. W., 1980: Stratocumulus-capped mixed layers derived from a three-dimensional model, Boundary-Layer Meteorol., 18, 495-527.

Kanda, M., Moriwaki, R., Kasamatsu, F., 2004: Large-eddy simulation of turbulent organized structures within and above explicitly resolved cube arrays, Boundary-Layer Meteorol., 112, 343-368.

Kanda, M., 2006: Large-eddy simulations on the effects of surface geometry of building arrays on turbulent organized structure, Boundary-Layer Meteorol., 118, 151-168.

Moureau, V., Berat, C., Pitsch, H., 2007: An efficient semi-implicit compressible solver for large-eddy simulations, J. Comput. Phys., 226, 1256-1270.

Tompkins, C. D., Adrian, R. J., 2003: Spanwise structure and scale growth in turbulent boundary layers, J. Fluid Mech., 490, 37-74.

Uehara, K., Murakami, S., Oikawa, S., Wakamatsu, S., 2000: Wind channel experiments on how thermal stratification affects flow in and above urban street canyons, Atmos. Env., 34, 1553-1562.